

# Wave Analysis of Multilayer Absorptive Low-Pass Interconnects

K. de Jager<sup>1,2</sup>, L. Dalessandro<sup>1,3</sup>, I. W. Hofsjager<sup>2</sup>, W. G. Odendaal<sup>1</sup>

<sup>1</sup> Center for Power Electronics Systems, Virginia Tech, USA

<sup>2</sup> Industrial Electronics Technology Research Group, University of Johannesburg, RSA

<sup>3</sup> Power Electronics Systems Laboratory, ETH Zurich, Europe

E-mails: kjager@vt.edu, dalessandro@IEEE.org, iwhofsajer@uj.ac.za, wgo@vt.edu

**Abstract**—The attenuation of EMI transmission line filters can be improved at high frequencies by employing eddy current absorption. This is achieved by introducing a material having a low conductivity and/or high permeability in specific regions of the conduction paths. In this paper the 1D propagation of a transverse electromagnetic (TEM) plane wave into conductive layers is modeled analytically and used to derive expressions for the field and current distributions in the metal. These results are the basis for computing the frequency dependent ohmic losses of the multi-layered conductive paths in the transmission line filter structures. They form part of a comprehensive analytical filter model, which is suitable for synthesis of integrated RF transmission line EMI filters.

**Keywords:** EMC, EMI, transmission line filters, wave propagation, eddy currents, skin effect, proximity effect, attenuation, ac resistance

## I. INTRODUCTION

The use of a distributed filter instead of just the conventional lumped discrete EMI filter at the interface between a converter and the mains supply is an attractive strategy for reducing the size of the input filter, or even replacing it [1]. Various implementations of such distributed filter structures have been investigated as in [2], [3] and [4]. In particular the distributed filter discussed in [4] made use of interconnects that have an inherent low-pass filtering characteristic. Through these interconnects the attenuation of the distributed filter was improved as shown for a converter application in [5]. However, up to now the precise mechanisms by which the interconnects improve the filter performance has only been understood heuristically in the broadest of terms. A formal treatment of the filter operation is needed for analysis and, more importantly, for filter synthesis.

The basic principles governing the filter's performance is directly related to the multi-layered geometry. There are two modes of operation that are of importance:

- a finite transmission line mode and
- an eddy current absorption mode.

The finite transmission line filtering mode can be analyzed using classical transmission line modeling methods, for instance by evolving the differential equations for an equivalent circuit comprised of distributed elements or per-unit length resistance, inductance, capacitance and conductance. An ideal transmission line filter is a lossless structure and the time

constants associated with the action of energy storage are responsible for damping certain frequencies, or in essence 'smoothing out' the undesired signals. This first mode of operation will be described in another article. In this paper we will limit the discussion solely to the second filtering mode, namely that of eddy current absorption.

The eddy current absorption mode is an improvement over the ideal lossless filter and uses the frequency dependent eddy current impedance of the structure to attenuate undesired noise signals by absorption, or, in other words, ohmic dissipation. In practice, this has been achieved by employing a multilayer conductor, where a low conductivity and/or high permeability material is added in the areas of current crowding. Such a conduction path can be thought of as a frequency selective conduction path, whereby the high frequency resistance (and impedance) in certain parts of the structure can be controlled by raising it in some areas.

### A. The Eddy Currents in a RF Transmission Line EMI Filter

In practice, both the CM (common mode) and the DM (differential mode) conducted EMI noise signals are filtered. Two transmission line attenuator structures are therefore used in the filter, namely a differential mode (DM) attenuator and a common mode (CM) attenuator, as shown schematically in Fig. 1 (a) and (b) respectively. Fig. 2 shows a photograph of a DM attenuator structure.

The dark squiggly lines in the schematic illustrates how the current might distribute in the metal layers as a function of penetration depth into the thickness of the structure. Current concentrates in areas of high magnetic field intensity and decays from there towards areas of low magnetic field intensity. In the rest of this paper, our focus shall only be on computing these eddy current distributions in these metal layers of the filter.

### B. Overview of the Proposed Modeling Procedure

In [6] Odendaal showed that the various 1D solutions for the eddy current distribution, including the solutions of Dowell in [7] as well as the orthogonal skin- and proximity effect equations in [8], in a current carrying strip conductor with

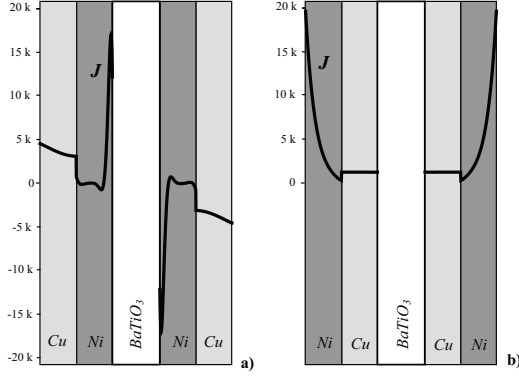


Fig. 1. Cross-section of (a) a DM attenuator and (b) a CM attenuator, indicating the current distribution in each as obtained using an eddy current FEM analysis.

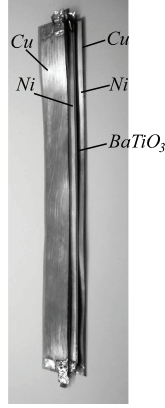


Fig. 2. A RF transmission line EMI filter being investigated.

arbitrary fields on its surfaces, are all equivalent, and that the skin- and proximity current distributions can be decoupled as well. Furthermore it was shown that the same structure can be analyzed by ignoring the current altogether and only considering the penetration of two known plane electromagnetic wave sources; one incident on each of the two conductor surfaces. This approach for deriving the eddy current effects for conductive layers uses the familiar TEM plane wave theory.

The analysis procedure that follows for the attenuator structures in question is an extension of the aforementioned method. The method is introduced by first considering an infinite slab of conductive material and then computing the electromagnetic field distributions due to radiation of electromagnetic plane waves into the metal, assuming angles of incidence that are perpendicular to the faces of the slab. The frequency dependent current distribution, which is responsible for the increase of the ac resistance as a function of frequency, is directly derived from the field solution of the Helmholtz equation. The model is then extended to two adjacent coplanar conductive slabs (which is found in the practical attenuator structures), each having a unique thickness, conductivity and permeability. For this approach to work properly, reflections at all the interface(s) of the slabs must also be accounted for. Once the current distribution has been found, the resistance of the conductive path and the attenuation of the structure

can be determined as functions of frequency. These analytical relationships will be combined with a comprehensive RF transmission line EMI filter model that describes the filter operation in its entirety.

## II. PREVIOUS 1D EDDY CURRENT MODELING METHODS

One of the most referenced eddy current modeling approaches suitable for transformer windings was written by Dowell [7] in 1966. In it he derived the current distribution inside a strip conductor without limitations on the value of the magnetic field on the conductor surface. The following solution was then obtained for the  $y = 0$  axis at the edge of a conductor having a thickness,  $h$ , and a width,  $w$ :

$$J_x(y) = \frac{\alpha I}{w} \left[ \frac{\cosh \alpha y}{\sinh \alpha h} - (k-1) \tanh \frac{\alpha h}{2} \cosh \alpha y + (k-1) \sinh \alpha y \right] \quad (1)$$

where

$$\alpha = \frac{1+j}{\delta} \quad (2)$$

and the *skin depth* is defined as follows:

$$\delta \equiv \frac{1}{\sqrt{\pi f \sigma \mu_0}} \quad (3)$$

The variable  $k$  is a real number associated with the magnitude of an external field. Ferreira [9] then recognized orthogonality between the skin- and proximity effect terms under the power integrals that has enabled mathematical decoupling of the dissipation sources. Subsequently, it was shown in [6] that the current distributions themselves can be decoupled as well. This result can be summarized by rewriting equation (1) as follows:

$$J_x = \frac{\alpha I \cosh \alpha y}{2w \sinh \frac{\alpha h}{2}} + \alpha H_s \frac{\sinh \alpha y}{\cosh \frac{\alpha h}{2}} \quad (4)$$

where the average magnetic field across the foil thickness is given by:

$$H_s = \frac{H_{s1} - H_{s2}}{2} = (2k-1) \frac{I}{2w} \quad (5)$$

and  $H_{s1}$  and  $H_{s2}$  are the two boundary values for magnetic field intensity. Note that the coordinate system has also been shifted so that  $y = 0$  is in the center of the conductor by replacing  $y$  with  $y + h/2$  in equation (1). It can be shown that (4) is identical to:

$$J_x = \left\{ \begin{array}{l} \underbrace{\alpha \left( \frac{H_{s2} - H_{s1}}{2} \right) \frac{\cosh \alpha y}{\sinh \frac{1}{2} \alpha h}}_{\text{skin effect component}} \\ + \\ \underbrace{\alpha \left( \frac{H_{s1} + H_{s2}}{2} \right) \frac{\sinh \alpha y}{\cosh \frac{1}{2} \alpha h}}_{\text{proximity effect component}} \end{array} \right. \quad (6)$$

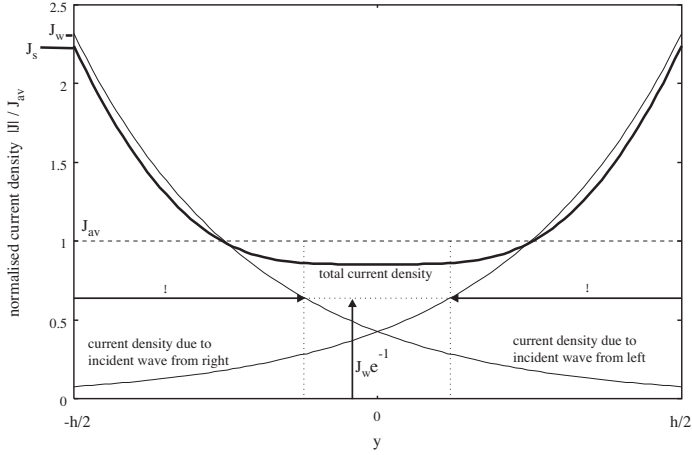


Fig. 3. The superposition of two inbound electromagnetic waves to obtain the current density distribution in the isolated foil conductor.

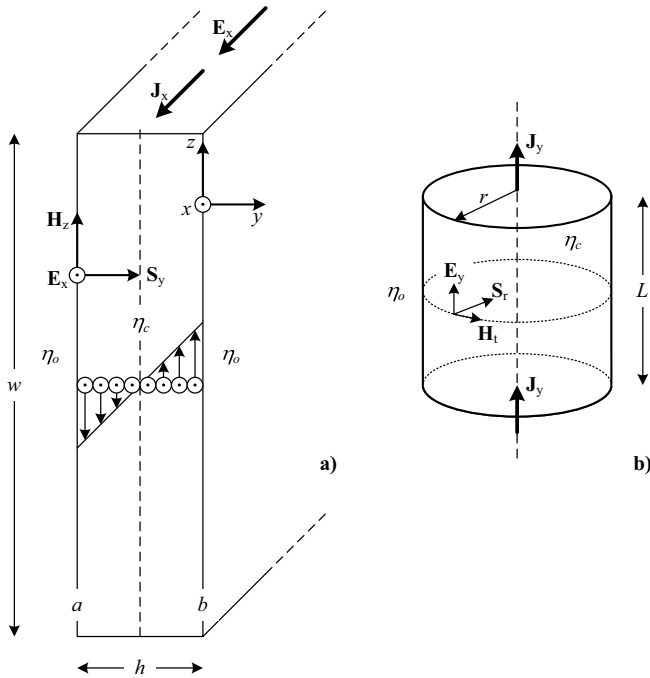


Fig. 4. (a) Cross-section of a conductive slab showing the direction of the electric and magnetic fields as well as the direction of propagation of the TEM wave. (b) The TEM wave for a conductor having circular cross-section propagates radially inwards.

In [6] it was further shown that the same result can also be obtained by superposition of two magnetic fields that penetrate the conductor from the opposing conductor surfaces (see Figure 3).

In the next sections we proceed with our analysis by modifying the above techniques to arrive at the eddy current solutions first for a single layer and then for the bi-layer metals that are found in the RF transmission line EMI filters.

### III. ABSORPTION IN A SINGLE-LAYER SLAB

In the analysis that follows it is essential to consider the current in a conductor not as a source, but as the result of electromagnetic waves penetrating into the conductor from the outside. The conduction current density distribution within the conductive slab is then likened to the currents induced due to the radiation of two coplanar waves in opposite directions into each of the two slabs.

Consider a single current-carrying conductor of rectangular cross-section, as shown in Fig. 4(a). The slab has a thickness,  $h$ , that is much smaller than its width,  $w$ . The electric field vector,  $\mathbf{E}_x$ , and the current density vector,  $\mathbf{J}_x$ , are known to be parallel to one another, as indicated by Ohm's Law:

$$\mathbf{J}_x = \sigma_c \mathbf{E}_x \quad (7)$$

where  $\sigma_c$  is the conductivity of the material. The direction of the internal magnetic field,  $\mathbf{H}_z$ , due to the current, can be determined using Ampere's Circuital Law. In so doing it can be seen that  $\mathbf{H}_z$  is tangential to the flat surfaces of the conductor at  $y = a = -h$  and  $y = b = 0$ . The direction of propagation of the associated electromagnetic wave corresponds with the direction of the complex Poynting vector, and is consequently seen to be along the  $y$ -axis, into the material (see Fig. 4).

$$\tilde{\mathbf{S}}_y = -\frac{1}{2} \tilde{\mathbf{E}}_x \times \tilde{\mathbf{H}}_z^* \quad (8)$$

Thus the current within the conductive slab can be considered in terms of waves that initially start on the interfaces of the slab and propagate into the material along the transverse  $y$ -direction. The same principle can be applied to a conductor having a circular cross-section, where the direction of propagation of the TEM wave, as given by the Poynting vector  $\mathbf{S}_r$ , is directed radially inwards (see Fig. 4(b)).

Assuming that the magnetic and electric fields only exhibit a dependence on the  $y$ -direction, the Helmholtz equation for the electric field intensity is then given by:

$$\frac{d^2 \tilde{\mathbf{E}}_x}{dy^2} + k^2 \tilde{\mathbf{E}}_x = 0 \quad (9)$$

Here we have limited our discussion to any harmonious frequency component, say  $\omega$  for all field quantities and we've indicated so by employing in our notation the tilde on top of vectors to identify them as phasor vectors. The solutions for these equations in the slab are:

$$\tilde{\mathbf{E}}(y) = \left( E_m^+ e^{-jk(y+h)} + E_m^- e^{jk(y+h)} \right) \mathbf{a}_x \quad (10)$$

$$\tilde{\mathbf{H}}(y) = \left( \frac{E_m^+}{\eta_c} e^{-jk(y+h)} - \frac{E_m^-}{\eta_c} e^{jk(y+h)} \right) \mathbf{a}_z \quad (11)$$

$E_m$  is the amplitude of the electric field at interface  $a$ , ( $\mathbf{a}_x, \mathbf{a}_y, \mathbf{a}_z$ ) are the unit vectors of the reference coordinate frame and

$$jk = \sqrt{j\omega\mu_c(\sigma_c + j\omega\epsilon_c)} \quad (12)$$

is known as the complex propagation constant. It is usual to write it as

$$jk = \gamma = \alpha_c + j\beta_c \quad (13)$$

where  $\alpha_c$  is the attenuation coefficient and  $\beta_c$  is the phase constant.

The characteristic impedances  $\eta_c$  of the conductive material and  $\eta_o$  of the air are given by:

$$\eta_c = \sqrt{\frac{j\omega\mu_c}{\sigma_c + j\omega\epsilon_c}}; \quad \eta_o = \sqrt{\frac{\mu_o}{\epsilon_o}}. \quad (14)$$

The time-domain fields are obtained using:

$$\mathbf{E}(y) = \text{Re}[\tilde{\mathbf{E}}(y)e^{j\omega t}]; \quad \mathbf{H}(y) = \text{Re}[\tilde{\mathbf{H}}(y)e^{j\omega t}] \quad (15)$$

where  $\omega = 2\pi f$  is the radian frequency of the alternating fields.

We now proceed to find the solution of the Helmholtz equation in a single slab conductor by distinguishing the electromagnetic wave as the source from the outside radiating into the metal. Our goal is to find the resulting current distribution inside the conductor with full consideration for transmission and reflection of waves at all the boundaries. The cross section of our slab is depicted in Fig. 4, and there is a wave incident from the left with a known value at boundary  $a$  given by:  $\tilde{\mathbf{H}}(-h)^- = \tilde{\mathbf{H}}_A$ . Since the wave is the source, reflections on the source side of the boundary must be omitted. On the right side of the boundary there is a transmitted wave comprising a wave propagating in the  $+y$  direction and a reflected wave propagating in the  $-y$  direction. The solution for the magnetic field is:

$$\tilde{H}_z(y) = \tilde{H}_{y0}^+ e^{-\alpha(y+h)} + \tilde{H}_{y0}^- e^{\alpha(y+h)} \quad (16)$$

The electric and magnetic fields at the boundary are tangential and continuous, so at  $y = -h$ :

$$\tilde{H}_A = \tilde{H}_{y0}^+ + \tilde{H}_{y0}^- \quad (17)$$

The wave propagating in the  $-y$  direction was reflected from the boundary at  $y = 0$  with a reflection coefficient

$$\Gamma = -\frac{\tilde{H}_{y0}^-}{\tilde{H}_{y0}^+} \quad (18)$$

Then we have

$$\tilde{H}_A = \tilde{H}_{y0}^+ - \Gamma \tilde{H}_{y0}^+ \quad (19)$$

If there is a source, say  $\tilde{H}_B$ , on the other side of the boundary at  $y = 0$ , then this reflection coefficient might as well include the incident wave in the  $-y$  direction due to the second source wave. At the other boundary at  $y = 0$  then:

$$\tilde{H}_B = \tilde{H}_{y0}^+ e^{-\alpha h} - \Gamma_S \tilde{H}_{y0}^+ e^{\alpha h} \quad (20)$$

where the subscript  $S$  is used to indicate that this is not just a conventional reflection coefficient, but one that includes a source. Solving for  $\Gamma_S$ , it is easily found as:

$$\Gamma_S = e^{-2\alpha h} - \frac{\tilde{H}_B}{\tilde{H}_A} e^{\alpha h} \quad (21)$$

In the special case where  $\tilde{H}_B = 0$ , this modified reflection coefficient becomes:

$$\Gamma_S = e^{-2\alpha h} \quad (22)$$

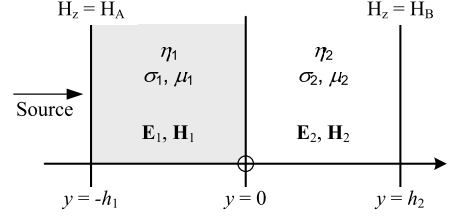


Fig. 5. The reflection and transmission of uniform plane waves as they propagate through two lossy media.

The current density as a function of penetration depth is found using  $\tilde{J}_x = \frac{\partial}{\partial y}(\tilde{H}_z)$ :

$$\tilde{J}_x(y) = -\alpha_1 \tilde{H}_{y0}^+ e^{-\alpha_1 y} - \alpha_1 \Gamma_S \tilde{H}_{y0}^+ e^{\alpha_1 y} \quad (23)$$

This equation represents the solution for a slab of material that has two magnetic field boundary values, one of which could be a source magnetic field intensity of 0 A/m. The result using a zero boundary is appropriate for geometries where symmetry could be forcing the MMF to be equal to zero on a boundary.

#### IV. ABSORPTION IN A BI-LAYER SLAB

In the next analysis another interface is introduced by considering, instead of a single slab of conductive material, two coplanar conductor slabs 1 and 2. The first and second slabs each owns a unique set of material properties  $\sigma_1, \mu_1, \alpha_1$  and  $\sigma_2, \mu_2, \alpha_2$ , respectively. For simplicity we'll assume that the frequency is low enough for us to ignore the effects of relative permittivity. As shown in Fig. 5, the problem is set up by placing the interface between the two slabs at position  $y = 0$  in our coordinate system. The left- and right-hand boundaries A and B are then at distances equal to the respective slab thicknesses,  $h_1$  and  $h_2$ . Once again we let the source be a wave that is incident from the left with a value  $\tilde{H}_{1z}(-h_1) = \tilde{H}_A$ . This time we'll first write the equation for the electric field intensity from the Helmholtz equation as:

$$\tilde{E}_{1x}(y) = \tilde{E}_{1x0}^+ e^{-\alpha_1(y+h_1)} + \Gamma_{12} \tilde{E}_{1x0}^+ e^{\alpha_1(y+h_1)} \quad (24)$$

The magnetic field in the first slab is then:

$$\tilde{H}_{1z}(y) = \frac{\tilde{E}_{1x0}^+}{\eta_1} e^{-\alpha_1(y+h_1)} - \Gamma_{12} \frac{\tilde{E}_{1x0}^+}{\eta_1} e^{\alpha_1(y+h_1)} \quad (25)$$

where

$$\eta_1 = \sqrt{\frac{j\omega\mu_1}{\sigma_1 + j\omega\epsilon_1}}$$

and

$$\eta_2 = \sqrt{\frac{j\omega\mu_2}{\sigma_2 + j\omega\epsilon_2}} \quad (26)$$

As before, we recognize that  $\Gamma_{12}$  is not the conventional reflection coefficient for an interface boundary (between slab 1 and slab 2), but that it has been modified to include the effects of wave sources elsewhere. The field solutions for the fields in the second slab are similar:

$$\tilde{E}_{2x}(y) = \tilde{E}_{2x0}^+ e^{-\alpha_2 y} + \Gamma_{23} \tilde{E}_{2x0}^+ e^{\alpha_2 y} \quad (27)$$

and the magnetic field in the second slab is:

$$\tilde{H}_{2z}(y) = \frac{\tilde{E}_{2x0}^+}{\eta_2} e^{-\alpha_2 y} - \Gamma_{23} \frac{\tilde{E}_{2x0}^+}{\eta_2} e^{\alpha_2 y} \quad (28)$$

where  $\Gamma_{23}$  is the modified reflection coefficient from the boundary at  $y = h_2$ . Symmetry allows us to limit our discussion to a source enforcing a magnetic field intensity equal to zero at that boundary, so that:

$$\tilde{H}_{3z}(y) = \tilde{H}_B = 0 \quad (29)$$

The boundary conditions produce the values of the four unknowns,  $\tilde{E}_{1x0}^+$ ,  $\tilde{E}_{2x0}^+$ ,  $\Gamma_{12}$ ,  $\Gamma_{23}$ , in four equations:

$$\begin{aligned} \tilde{E}_{1x0}^+ (e^{-\alpha_1 h_1} + \Gamma_{12} e^{\alpha_1 h_1}) &= \tilde{E}_{2x0}^+ (1 + \Gamma_{23}) \\ \frac{\tilde{E}_{1x0}^+}{\eta_1} (e^{-\alpha_1 h_1} - \Gamma_{12} e^{\alpha_1 h_1}) &= \frac{\tilde{E}_{2x0}^+}{\eta_2} (1 - \Gamma_{23}) \\ \frac{\tilde{E}_{1x0}^+}{\eta_1} (1 - \Gamma_{12}) &= \tilde{H}_A \end{aligned}$$

$$\frac{\tilde{E}_{2x0}^+}{\eta_2} (e^{-\alpha_2 h_2} - \Gamma_{23} e^{\alpha_2 h_2}) = 0$$

The simultaneous solution of these four equations is the only remaining step for completing the solution. The modified reflection coefficients are:

$$\begin{aligned} \Gamma_{23} &= e^{-2h_2 \alpha_2} \\ \Gamma_{12} &= \frac{e^{-2h_1 \alpha_1} (-\eta_1 (e^{-2h_2 \alpha_2} - 1) + \eta_2 (e^{2h_2 \alpha_2} + 1))}{\eta_1 (e^{2h_2 \alpha_2} - 1) + \eta_2 (e^{2h_2 \alpha_2} + 1)} \end{aligned}$$

## V. COMPARISON OF NUMERICAL AND ANALYTICAL RESULTS IN CASE STUDIES

In practice, it is almost impossible to directly measure current distributions. Normally a current distribution can only be inferred from a resistance measurement which makes it difficult to experimentally confirm the results of an analytical model. FEM (finite element modeling) was therefore used to examine the validity of the model and to investigate the frequency dependencies of the fields.

### A. FEM Comparison for the Single Layer Metal

The results for the single conductive slab can be broken up into two cases, namely the field distributions as a result of skin effect only and as a result of skin and proximity effects. In the first case the external magnetic field was set equal to zero. The field distributions predicted by the model exhibit excellent correlation with the FEM results for a copper slab, as shown in Figures (6) and (7). Note that the results were tested for three frequencies, namely 1kHz, 10kHz and 100kHz. The distribution predicted by the model is represented by the solid lines while the dashed lines give the distributions obtained using FEM.

For the second case the external magnetic field components took on some value due to the presence of a second conductive slab in close proximity to the original slab. In the FEM

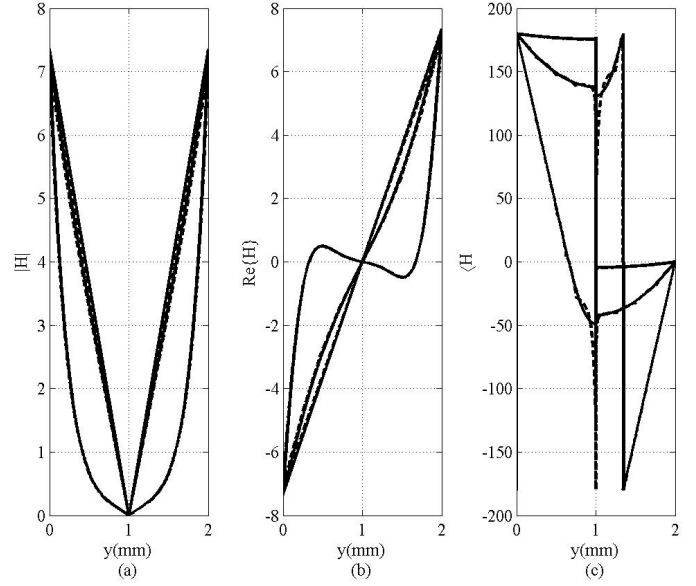


Fig. 6. (a) Magnitude, (b) real part and (c) phase of  $\mathbf{H}$ , due to the skin effect only, for three different frequencies

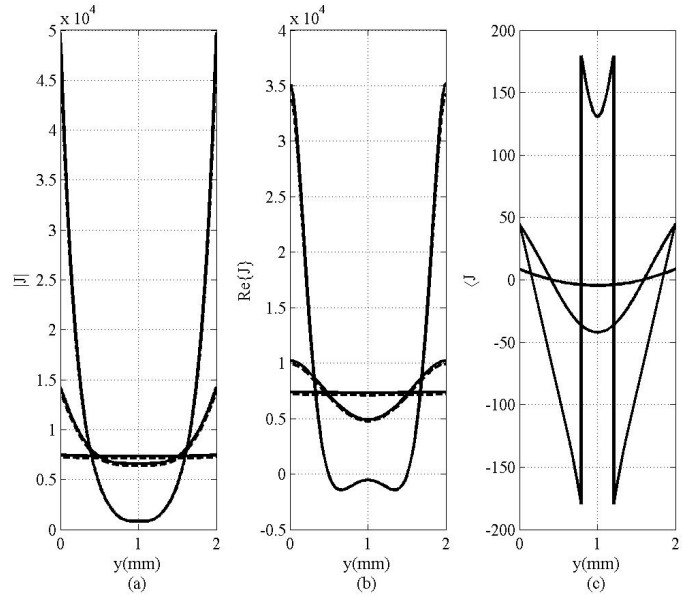


Fig. 7. (a) Magnitude, (b) real part and (c) phase of  $\mathbf{J}$ , due to the skin effect only, for three different frequencies

environment this was realized by adding a second slab, which was identical to the first. This creates a situation where the single conductive slab is in the presence of a uniform magnetic field with amplitude equal to the surface magnetic field of a single conductive slab with no external magnetic field. The exact value of the external field is:

$$\tilde{H}_{s_{ext}} = \frac{-I}{2w} \quad (30)$$

Once again the field distributions predicted by the model showed excellent correlation with the FEM results as shown in Figures (8) and (9).

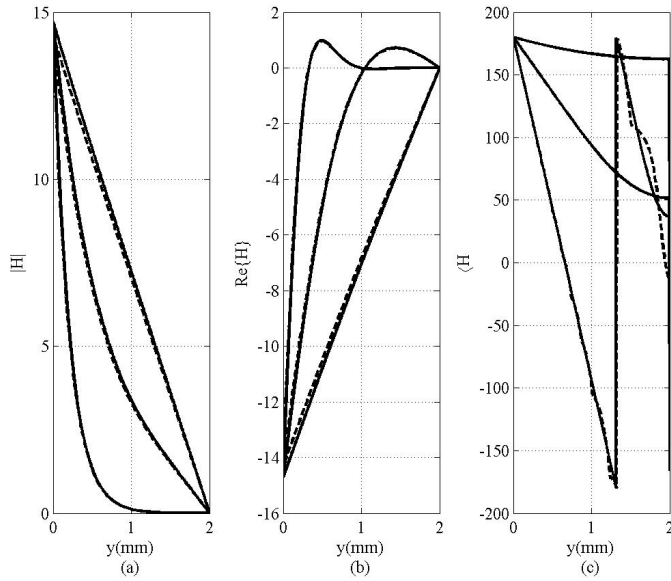


Fig. 8. (a) Magnitude, (b) real part and (c) phase of  $\mathbf{H}$ , due to the skin and proximity effect, for three different frequencies

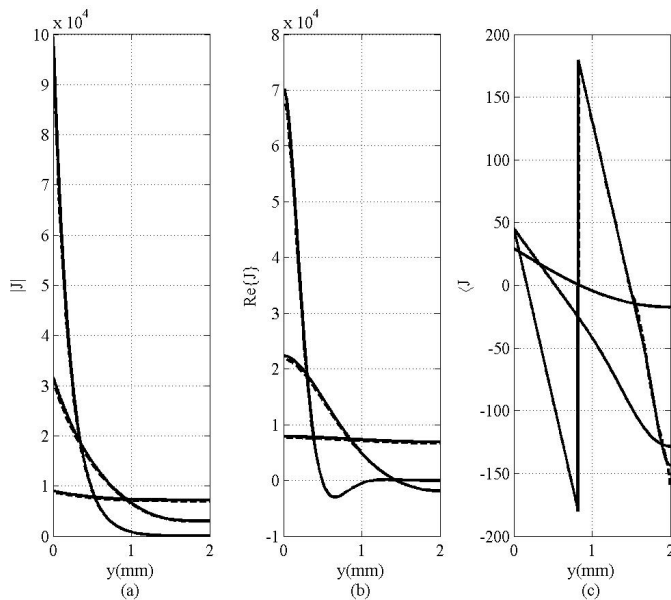


Fig. 9. (a) Magnitude, (b) real part and (c) phase of  $\mathbf{J}$ , due to the skin and proximity effect, for three different frequencies

### B. FEM Comparison for the Bi-Layer Metal

The analytical results for the field distributions in a bi-layer slab will now be compared to results obtained using finite element simulation software. In the practical filters the relative thicknesses and skin depths of copper and nickel produce a very sharp decay of field quantities in the nickel layers. This decay is so fast that it is virtually impossible to make a good judgement when attempting to compare the results to the finite element solutions. For this reason the dimensions and the material properties of the metal layers were adjusted so that the field distributions are more pronounced and exaggerated for

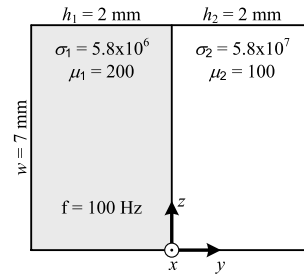


Fig. 10. The dimensions and material properties of a bi-layer slab for comparison with FEM.

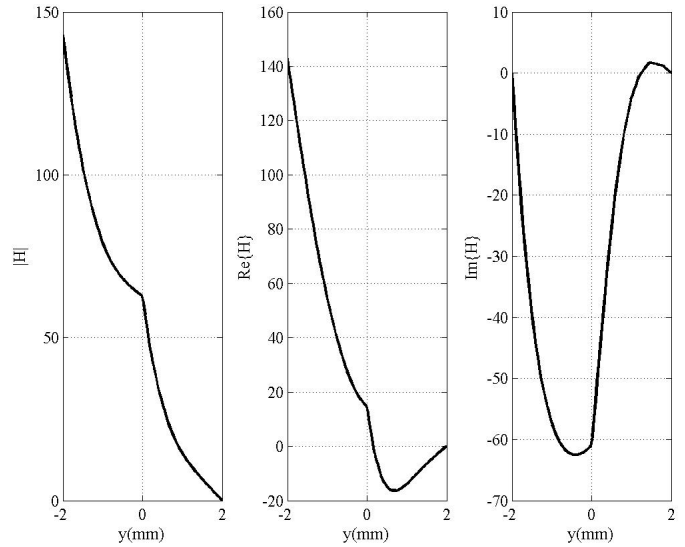


Fig. 11. The analytical and FEM results for the magnetic field intensity as a function of penetration depth for the bi-layer example.

easy comparison. Fig. 10 depicts the dimensions and material properties of the chosen bi-layer slab conductor. The source field is incident from the left boundary and the current flows out of the page.

The analytical results of the magnetic field intensity and current density distributions are shown together with FEM results in Figure 11 and Figure 12, respectively. There is only one line in each of the plots, because there is precise agreement between the analytical solutions and the results from FEM.

## VI. EDDY CURRENT RESISTANCE

The analytical solution for the current distribution can be used to find the per-unit-length high frequency resistance (31). The results for the single conductive slab are shown in Fig. 13.

$$R_{ac} = \frac{w}{2\sigma_c} \int_0^h \mathbf{J} \cdot \mathbf{J}^* dz \quad (31)$$

Fig. 14 depicts the ac to dc resistance ratio for test case A, the bi-layer case study in the previous section, as a function of frequency. Test case B is the result for another bi-layer structure which comprises a 2mm sheet of copper that has been metalized on one side with a 200 $\mu$ m thick layer of nickel.

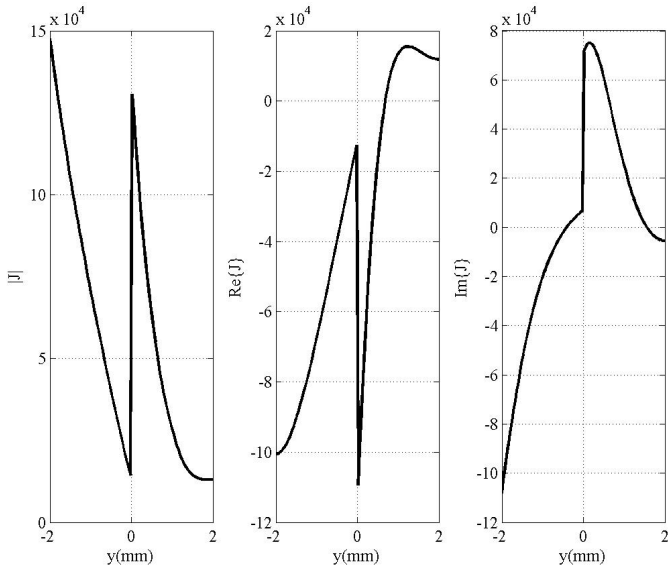


Fig. 12. The analytical and FEM results for the current density as a function of penetration depth for the bi-layer example.

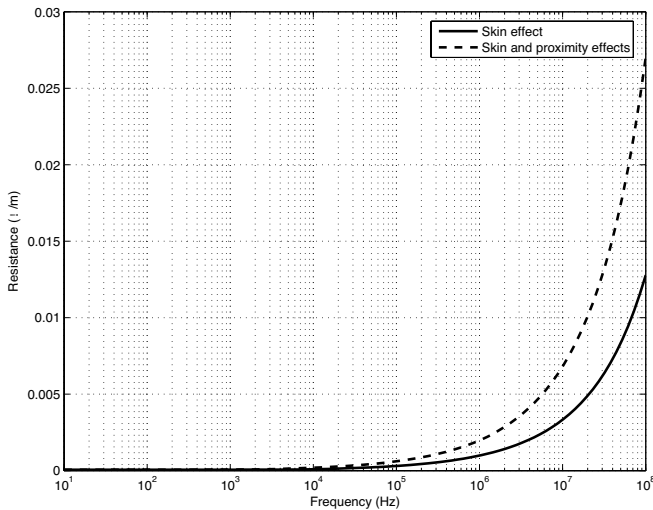


Fig. 13. Frequency dependence per-unit-length resistance of the single conductive slab due to skin effect alone and due to skin and proximity effects.

## VII. CONCLUSION

A method for modeling the field distributions in multi-layered conductive slabs was presented. It is based on the radiation of electromagnetic plane waves into flat conductive slabs. This analytical model correlates precisely with the 1D field distributions obtained using FEM for single and bi-layer conductive slabs. The analysis can also be extended to more

conductive layers with the same procedure, however more layers are not necessary for the transmission line filter application. The model enables the extraction of the frequency dependent resistances and impedances of the conductive layers. This modeling technique forms part of a more comprehensive analytical model of the RF transmission line EMI filter structures, which includes the finite transmission line mode of filtering.

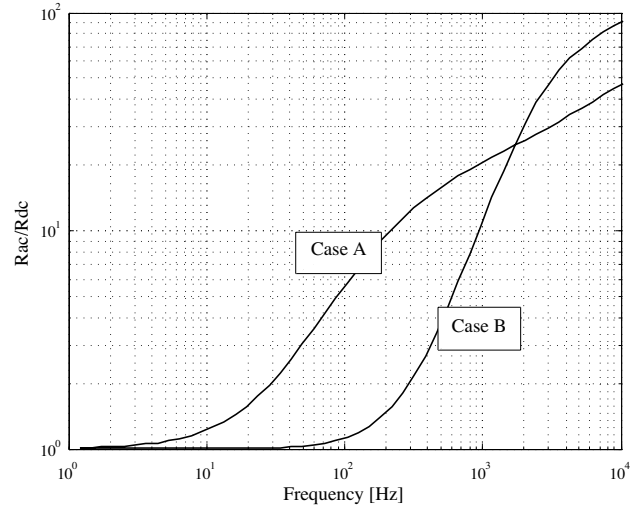


Fig. 14. The AC to DC resistance ratios for two bi-layer case studies as functions of frequency.

## VIII. ACKNOWLEDGMENT

Ansoft Maxwell was used to perform all the 2D Finite Element simulations.

## REFERENCES

- [1] J. H. Bogar and E. M. Reyner, "Miniature low-pass EMI filters," *Proc. of the IEEE*, vol. 67, pp. 159–163, January 1979.
- [2] H. M. Schlicke and H. Weidman, "Compatible EMI filters," *IEEE Spectrum*, pp. 59–68, October 1967.
- [3] J. D. van Wyk jr, W. A. Cronje, J. D. van Wyk, P. J. Wolmarans, and C. K. Campbell, "Integrated power filters utilizing skin- and proximity effect based low-pass interconnects," *Proc. of Conf. on Integrated Power Electronics Systems*, pp. 73–82, June 2002.
- [4] L. Zhao, R. Chen, and J. van Wyk, "An integrated common mode and differential mode transmission line RF-EMI filter," *Proc. of Power Electronics Specialists Conference*, pp. 4522–4526, 2004.
- [5] A. C. Baisden, D. Boroyevich, and J. D. van Wyk, "High frequency modeling of a converter with an RF-EMI filter," *Proc. of Industry Applications Conference*, vol. 5, pp. 2290–2295, October 2006.
- [6] W. G. Odendaal, "A generic approach for the modelling of high power density magnetic components," *Ph.D dissertation, Rand Afrikaans University*, May 1997.
- [7] P. L. Dowell, "Effects of eddy currents in transformer windings," *Proc. of the IEE*, vol. 113, pp. 1387–1394, August 1966.
- [8] R. L. Stoll, "The analysis of eddy currents," Oxford University Press, London, 1974.
- [9] J. A. Ferreira, *Electromagnetic Modelling of Power Electronic Converters*. MA, USA: Kluwer Academic Publishers, 1989.